Supplemental Figures

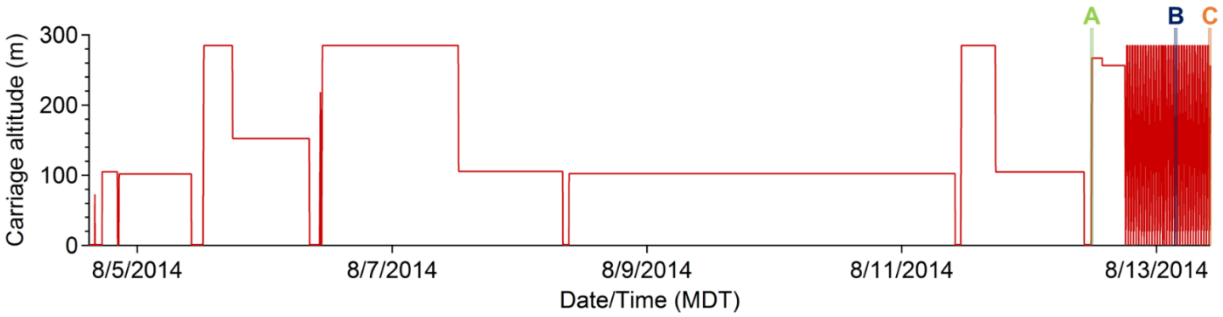

Figure S1. Timeseries of tower elevator carriage altitude throughout the reported measurement period. Representative noon, night, and morning vertical profiles were measured at the periods denoted 'A', 'B', and 'C', respectively.

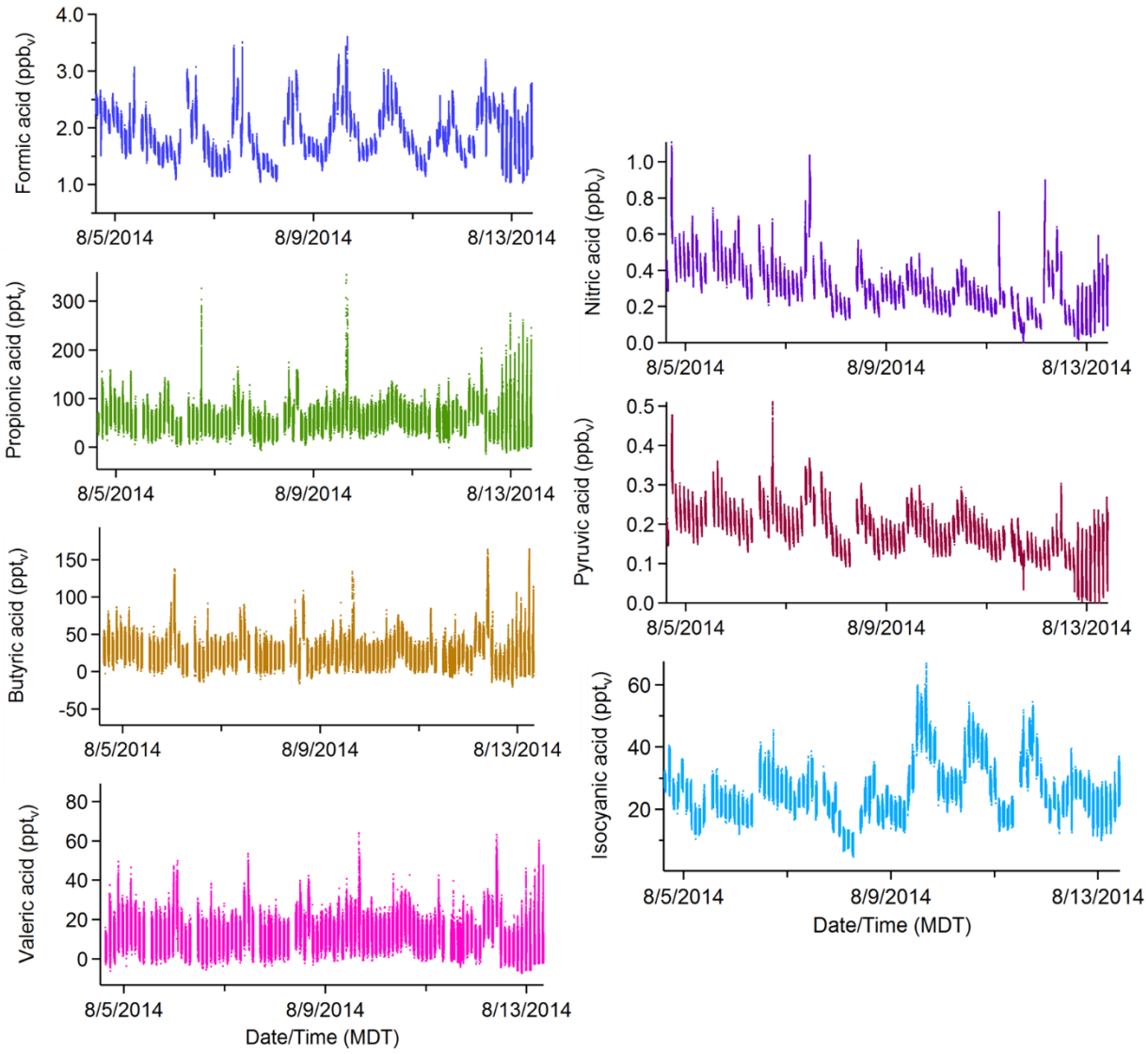

Figure S2. Mixing ratio data timeseries for all detected gas-phase acids spanning the reported data acquisition period. All data were collected at 1 Hz acquisition rates.

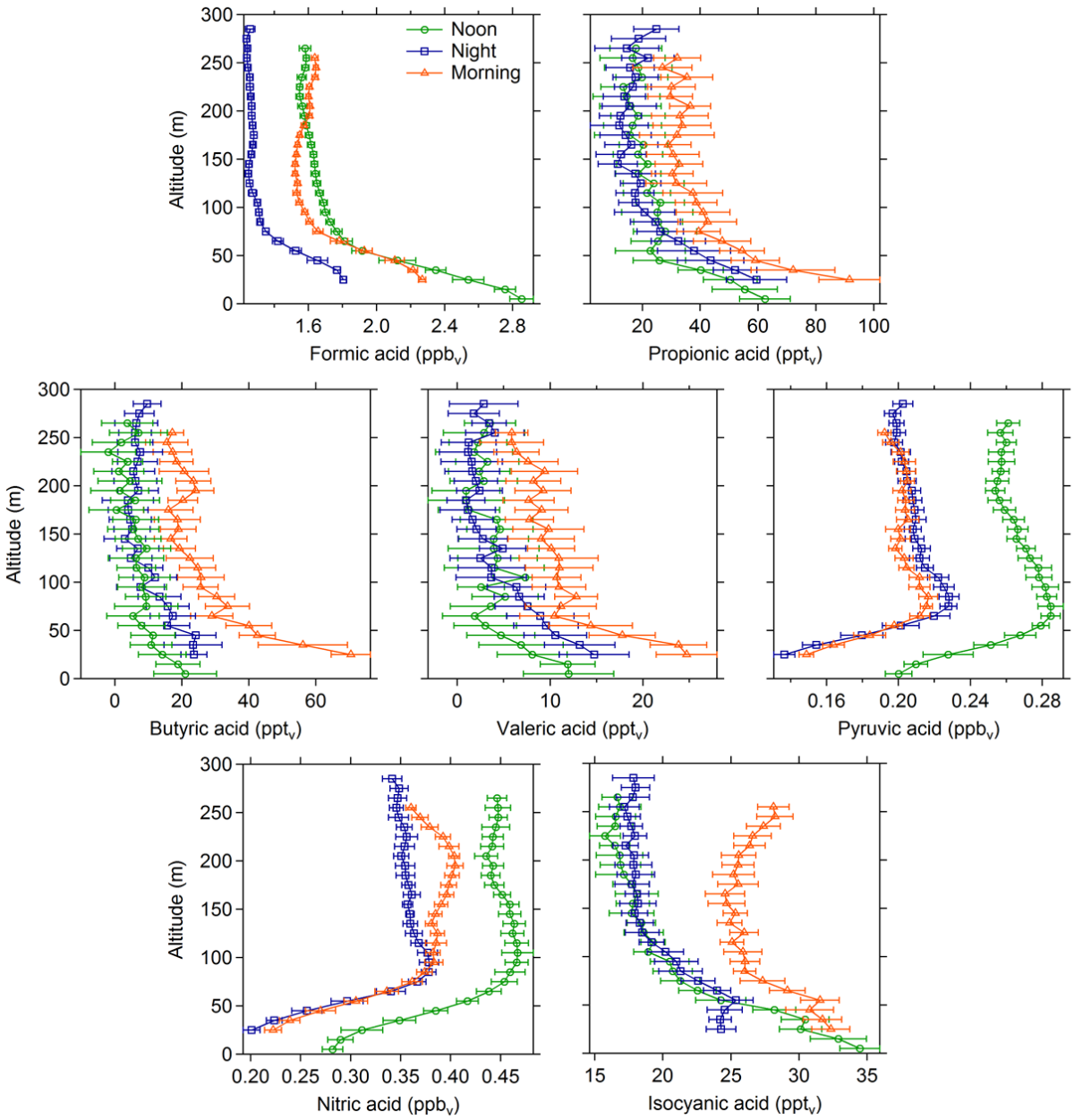

Figure S3. Vertical profiles for all detected gas-phase acids at representative noon, night, and morning periods, showing mixing ratios as a function of altitude. Data are binned by altitude (10 m per bin). Data points are means of each bin. Error bars represent ± one standard deviation of binned values.

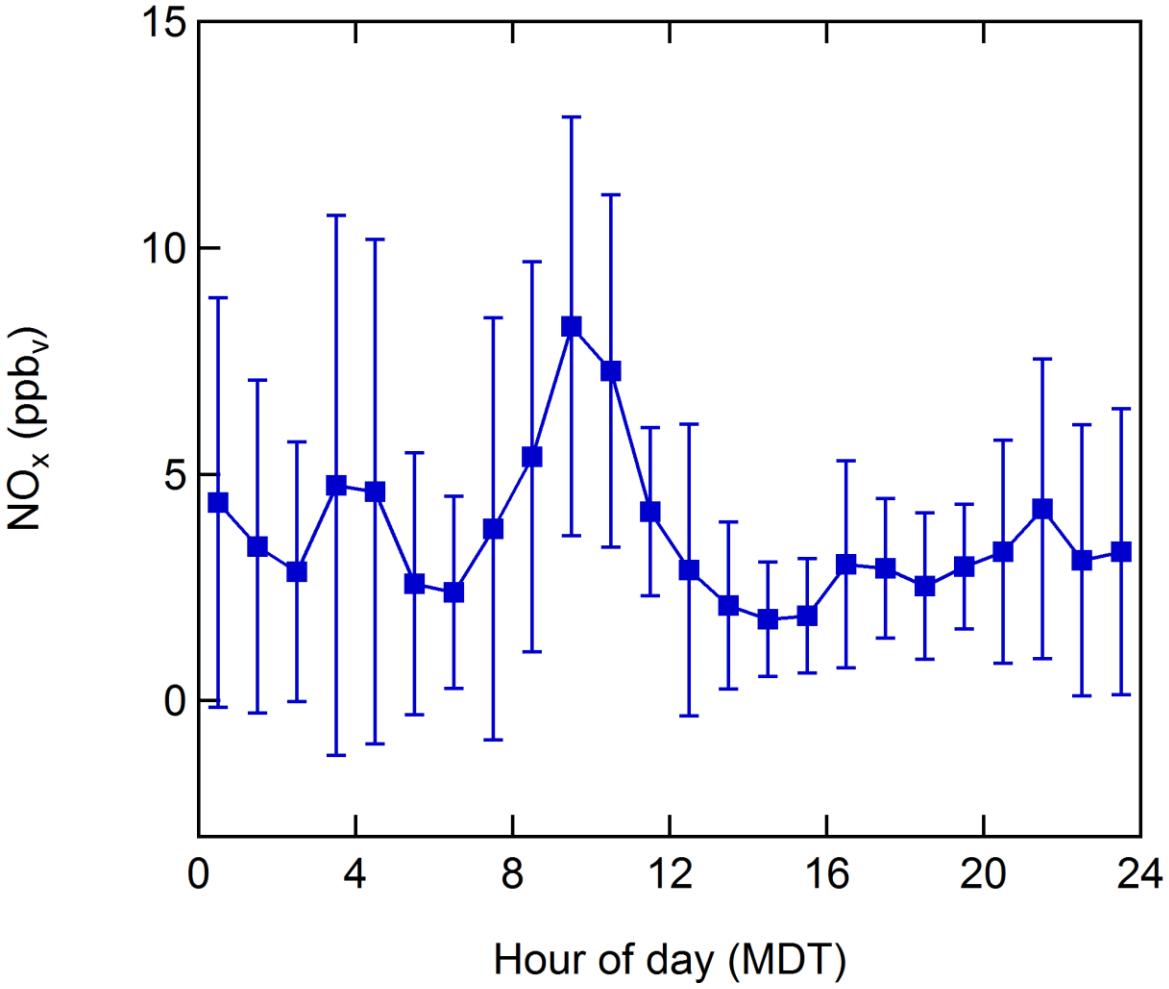

Figure S4. Diel profile of NO_x measured at the site throughout the reported measurement period. Data are binned by hour of day. Data points are binned means, and error bars are ± one standard deviation of binned data.

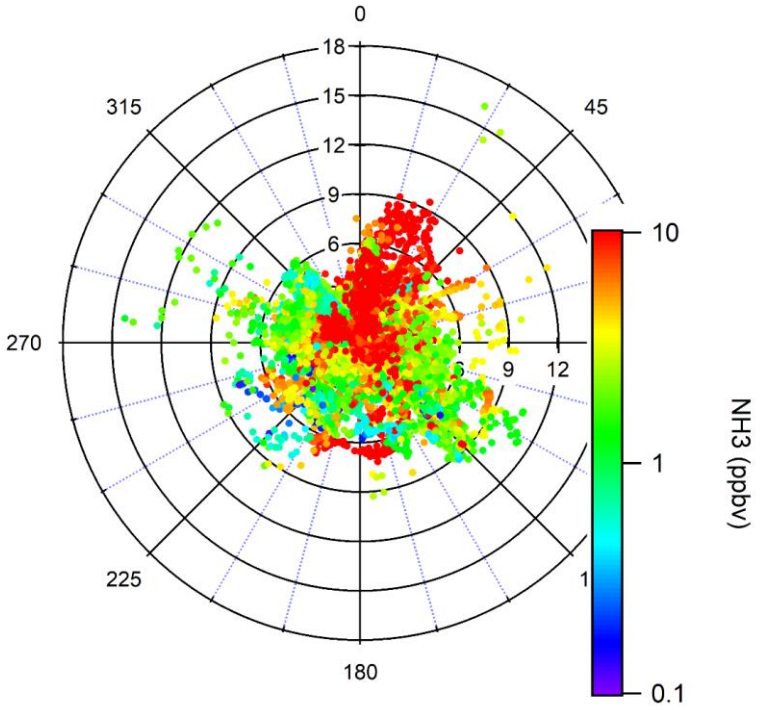

Figure S5. Wind plot of ammonia measured at the BAO tower during the reported measurement period. Data points are colored by mixing ratio. Angular axis corresponds to wind direction (degrees), with 0, 90, 180, and 270 degrees corresponding to N, E, S, and W cardinal directions, respectively. Radial axes correspond to wind speed (m s^{-1}).

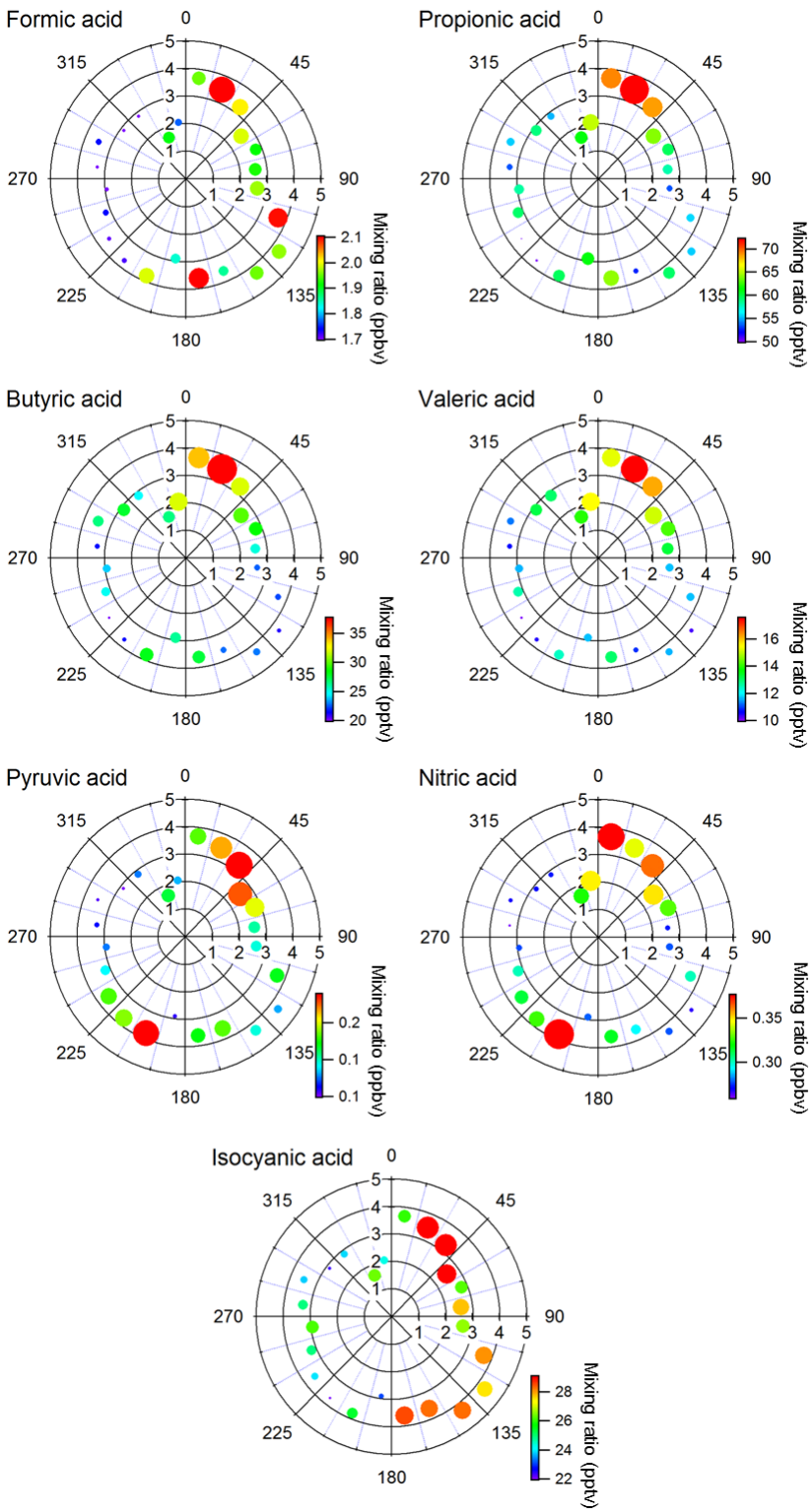

Figure S6. Radial plots with wind speed (m s^{-1}), direction (degrees), and acid mixing ratio data binned into 15° angular bins. Degrees correspond to cardinal directions (i.e. 0° is N, 90° is E, etc.). Radial positions of markers represent the diel average wind speed within each angular bin. Markers are colored and sized by the diel average mixing ratio of each acid within each angular bin.

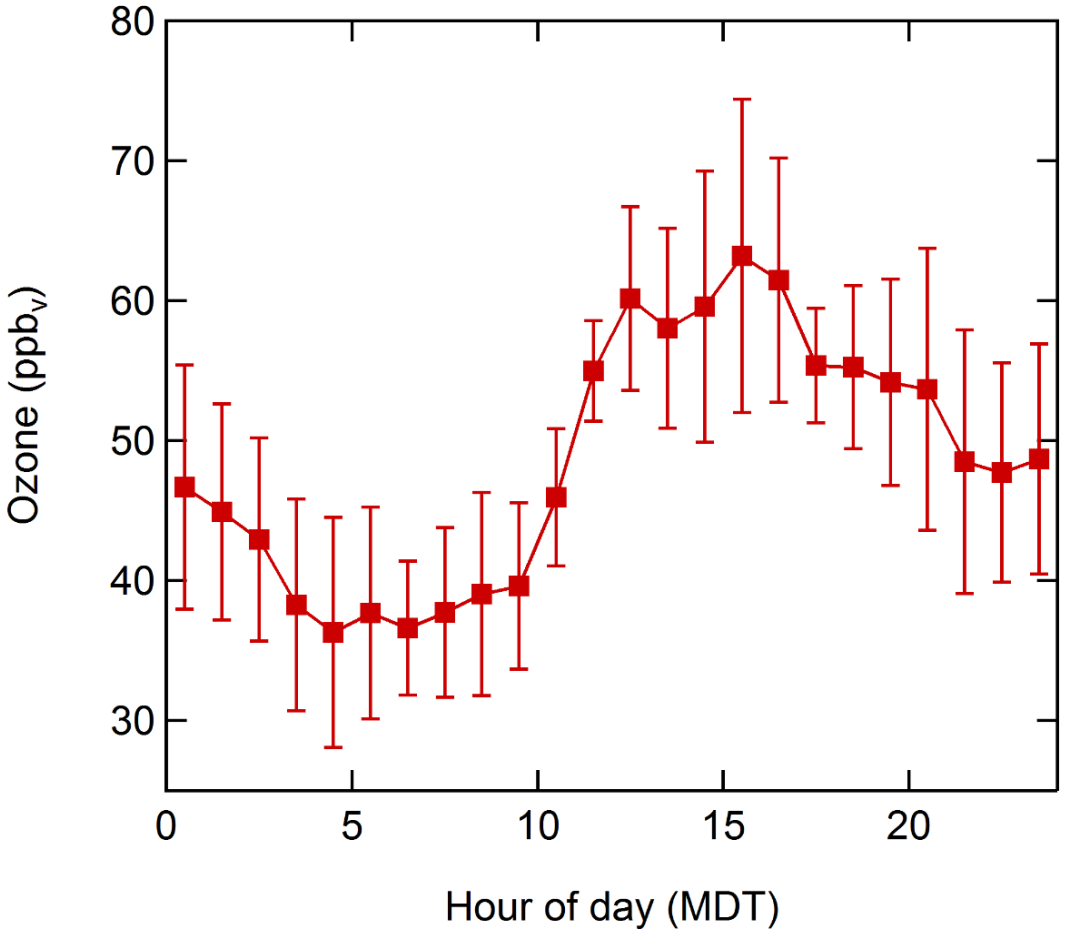

Figure S7. Diel profile of ozone measured at the site throughout the reported measurement period. Data are binned by hour of day. Data points are binned means, and error bars are ± one standard deviation of binned data.

Supplemental Discussion

In-laboratory gas-phase acid calibrations and FRAPPE sensitivity estimations

The calibration setup shown in Figure S7 was recreated in a laboratory setting, with the heated calibration oven containing permeation standards of all gas-phase acid compounds presented here. External standard calibrations of these compounds were performed to determine ToF-CIMS sensitivities of these compounds. A sensitivity-ratio estimation was employed to estimate instrumental sensitivity of these compounds during the FRAPPE campaign:

$$S_{x,FRAPPE} = \frac{S_{X,lab}}{S_{FA,lab}} \cdot S_{FA,FRAPPE}$$

where $S_{x,FRAPPE}$ is the estimated sensitivity of a given gas-phase compound during FRAPPE, $S_{x,lab}$ is the measured sensitivity of a given gas-phase compound from in-lab calibrations, $S_{FA,lab}$ is the measured sensitivity of formic acid from in-lab calibrations, and $S_{FA,FRAPPE}$ is the mean sensitivity of formic acid during FRAPPE. A table of estimated sensitivity values for all gas-phase species measured during FRAPPE is provided below.

Gas-phase acid	Propionic	Butyric	Valeric	Pyruvic	Nitric	Isocyanic
Est. Sensitivity (ncps/ppbv)	2590	4700	6300	20400	24000	85900

Estimating NH_4NO_3 aerosol formation as sink for HNO_3

Reactions between gas-phase HNO_3 and NH_3 produce NH_4NO_3 aerosol, and therefore act as a potential tropospheric sink for gas-phase HNO_3. Gas-particle phase partitioning is an equilibrium process that depends on ambient temperature and relative humidity (RH) (Seinfeld and Pandis, 1998; Li et al., 2014). Methods for estimating NH_4NO_3 formation from HNO_3 and NH_3 are outlined by Seinfeld and Pandis (1998). Deliquescence relative humidity (DRH) can be calculated by the following:

$$\ln(DRH) = \frac{723.7}{T} + 1.6954$$

Ambient RH at the site was below the DRH for > 90% data reported here, indicating that most NH_4NO_3 produced was in the solid phase. Neglecting aqueous phase aerosol production allows for a simplified estimation of NH_4NO_3 partitioning (as previously performed by Li et al. (2014)), which can be expressed by the following equilibrium expression:

$$NH_4NO_3(s) \rightleftharpoons NH_3(g) + HNO_3(g)$$

and the accompanying equilibrium constant is therefore given by:

$$K = [NH_3][HNO_3]$$

where [NH_3] and [HNO_3] are the gas-phase mixing ratios of NH_3 and HNO_3, respectively. The expected equilibrium constant, K_p, is calculated by:

$$\ln(K_p) = 84.6 - \frac{24200}{T} - 6.1 \times \ln\left(\frac{T}{298}\right)$$

where T is ambient temperature. Solid NH_4NO_3 formation is favorable when $K > K_p$—i.e. when the system is supersaturated with NH_3 and HNO_3. $K > K_p$ for < 10% for the data reported here, indicating that NH_4NO_3 formation was predominantly unfavorable, and therefore suggesting that this process does not serve as a major sink of gas-phase HNO_3. NH_4NO_3 formation is typically less favorable when RH is low and temperature is high (Li et al., 2014), as is the case for a typical summer day in the Front Range.

Estimating aqueous-phase partitioning of gas-phase acids

Aqueous-phase partitioning was evaluated as a potential sink for gas-phase acids by using Henry's Law:

$$H_x = \frac{[X]_{aq}}{P_x}$$

where H_x is the Henry's Law constant for a given gas-phase acid, and $[X]_{aq}$ and P_x are the aqueous concentration and partial pressure of said acid species, respectively. P_x was calculated by gas-phase acid mixing ratio data, as well as meteorological data collected during the campaign. Moles of a given acid in the aqueous-phase was determined by $[X]_{aq}$ and ambient liquid water concentration (LWC). LWC in the Front Range during the summer is estimated to be around 1 μg m^{-3}, based on continental estimates of LWC reported by Carlton and Turpin (2013). Combining aqueous-phase moles of a given acid with the ideal gas law, and meteorological data from the site yields a total loss of said acid from the gas-phase through partitioning. This estimation is limited in that it does not account for the effects of pH or other dissolved ions of a given acid's solubility, but we would not expect a change of several orders of magnitude by accounting for these effects.

Supplemental References

Carlton, A., and Turpin, B.: Particle partitioning potential of organic compounds is highest in the Eastern US and driven by anthropogenic water, Atmospheric Chemistry and Physics, 13, 10203-10214, 2013.

Li, Y., Schwandner, F. M., Sewell, H. J., Zivkovich, A., Tigges, M., Raja, S., Holcomb, S., Molenar, J. V., Sherman, L., and Archuleta, C.: Observations of ammonia, nitric acid, and fine particles in a rural gas production region, Atmospheric environment, 83, 80-89, 2014.

Seinfeld, J. H., and Pandis, S. N.: Atmospheric Chemistry and Physics, 1 ed., Wiley-Interscience, Canada, 1998.